Published in final edited form as:
J Comp Neurol. 2013 January 1; 521(1): 109–129. doi:10.1002/cne.23164.

Postnatal Development of Brain-Derived Neurotrophic Factor (BDNF) and Tyrosine Protein Kinase B (TrkB) Receptor Immunoreactivity in Multiple Brain Stem Respiratory-Related Nuclei of the Rat

Qiuli Liu and **Margaret T.T. Wong-Riley***
Department of Cell Biology, Neurobiology and Anatomy, Medical College of Wisconsin, Milwaukee, Wisconsin, 53226

Abstract

Previously, we found a transient imbalance between suppressed excitation and enhanced inhibition in the respiratory network of the rat around postnatal days (P) 12–13, a critical period when the hypoxic ventilatory response is at its weakest. The mechanism underlying the imbalance is poorly understood. Brain-derived neurotrophic factor (BDNF) and its tyrosine protein kinase B (TrkB) receptors are known to potentiate glutamatergic and attenuate gamma-aminobutyric acid (GABA)ergic neurotransmission, and BDNF is essential for respiratory development. We hypothesized that the excitation-inhibition imbalance during the critical period stemmed from a reduced expression of BDNF and TrkB at that time within respiratory-related nuclei of the brain stem. An in-depth, semiquantitative immunohistochemical study was undertaken in seven respiratory-related brain stem nuclei and one nonrespiratory nucleus in P0–21 rats. The results indicate that the expressions of BDNF and TrkB: 1) in the pre-Bötzinger complex, nucleus ambiguus, commissural and ventrolateral subnuclei of solitary tract nucleus, and retrotrapezoid nucleus/parafacial respiratory group were significantly reduced at P12, but returned to P11 levels by P14; 2) in the lateral paragigantocellular nucleus and parapyramidal region were increased from P0 to P7, but were strikingly reduced at P10 and plateaued thereafter; and 3) in the nonrespiratory cuneate nucleus showed a gentle plateau throughout the first 3 post-natal weeks, with only a slight decline of BDNF expression after P11. Thus, the significant downregulation of both BDNF and TrkB in respiratory-related nuclei during the critical period may form the basis of, or at least contribute to, the inhibitory-excitatory imbalance within the respiratory network during this time.

Keywords

commissural and ventrolateral subnuclei of the solitary tract nucleus; critical period; lateral paragigantocellular nucleus; nucleus ambiguus; pre-Bötzinger complex; retrotrapezoid nucleus/parafacial respiratory group

*CORRESPONDENCE TO: Department of Cell Biology, Neurobiology, and Anatomy, Medical College of Wisconsin, 8701 Watertown Plank Road, Milwaukee, WI 53226. mwr@mcw.edu.

CONFLICT OF INTEREST Both authors declare no competing financial interests.

ROLE OF AUTHORS Both authors had full access to all the data in the study and take responsibility for the integrity of the data and the accuracy of the data analysis.

Previously, we found a transient imbalance between heightened expression of inhibitory neurochemicals and suppressed expression of excitatory neurochemicals in multiple brain stem nuclei within the respiratory network of the rat at postnatal days (P) 12–13, a critical period of respiratory development when the animals' ventilatory and metabolic responses to hypoxia are at their weakest (Liu and Wong-Riley, 2002, 2003, 2005; Wong-Riley and Liu, 2005, 2008; Liu et al., 2006, 2009). The mechanism underlying this imbalance, demonstrable at the electrophysiological level (Gao et al., 2011), is poorly understood.

Brain-derived neurotrophic factor (BDNF) and its high affinity receptor, tyrosine protein kinase B (TrkB) receptor, play important roles in neuronal cell survival, differentiation, cell migration, neurite outgrowth, synapse formation, stabilization, and plasticity (Hofer and Barde, 1988; Wardle and Poo, 2003; Baker-Herman et al., 2004; Yoshii and Constantine-Paton, 2010). They reportedly regulate inhibitory-excitatory imbalance in the nervous system by enhancing glutamatergic neurotransmission and attenuating gamma-aminobutyric acid (GABA)ergic and glycinergic ones (Wardle and Poo, 2003; Bardoni et al., 2007). Importantly, BDNF-TrkB signaling is essential for the development of brain stem respiratory system (Erickson et al., 1996; Katz, 2005; Ogier et al., 2007) and their disruption presumably contribute to severe respiratory dysfunction in Rett's syndrome (Katz, 2005; Ogier et al., 2007; Katz et al., 2009), an X-linked neurodevelopmental disorder. BDNF and TrkB are expressed in respiratory neurons (Thoby-Brisson et al., 2003; Katz, 2005) and their expressions are reportedly developmentally regulated (Kaisho et al., 1991; Kim et al., 2007; Bartkowska et al., 2010). However, to date virtually nothing is known about the developmental expressions of BDNF and TrkB in brain stem respiratory-related nuclei.

Based on the importance of BDNF and TrkB in respiratory development and in neurotransmission, we hypothesize that the excitatory-inhibitory imbalance observed in brain stem respiratory-related nuclei during the critical period stemmed from a reduced expression of BDNF and TrkB at that time. We therefore conducted an in-depth, immunohistochemical and single neuron optical densitometric analysis of BDNF and TrkB receptors in seven respiratory-related nuclei and one nonrespiratory nucleus of P0–21 rats: the pre-Bötzinger complex (PBC, a presumed center or kernel for respiratory rhythmogenesis (Smith et al., 1991, 2000; Rekling and Feldman, 1998)); nucleus ambiguus (Amb, which innervates airway muscles of the pharynx and larynx and receives input from the central respiratory network (Jordan, 2001)); commissural and ventrolateral subnuclei of the solitary tract nucleus (NTS_{COM} and NTS_{VL}, both receive direct projections from peripheral chemoafferent fibers (Finley and Katz, 1992), and both are part of the dorsal respiratory group known to project to the ventral respiratory group (Smith et al., 1989; Holtman et al., 1990; Bonham, 1995)); retrotrapezoid nucleus/parafacial respiratory group (RTN/pFRG, known to be involved in central chemoreception (Guyenet et al., 2005) and is reportedly a second oscillator in neonatal and juvenile rodents and perhaps a conditional oscillator that controls active expiration (Onimaru and Homma, 2003; Feldman, 2011)); and the lateral paragigantocellular nucleus and parapyramidal region (LPGi and pPy, both have extensive connections with the dorsal and ventral respiratory groups (Smith et al., 1989; Zec and Kinney, 2001; Cream et al., 2002; Ribas-Salgueiro et al., 2005)). The nonrespiratory cuneate nucleus (CN) is a relay in the somatosensory system with no known respiratory function and served as an internal control.

MATERIALS AND METHODS

Tissue preparation

All experiments and animal procedures were performed in accordance with the *Guide for the Care and Use of Laboratory Animals* (National Institutes of Health Publication No. 80-23, revised 1996), and all protocols were approved by the Medical College of Wisconsin

Animal Care and Use Committee (approval can be provided upon request). All efforts were made to minimize the number of animals used and their suffering.

A total of 138 Sprague–Dawley rats, both male and female, from 11 litters were used. Rat pups were sacrificed at each of P0, 2, 3, 4, 5, 7, 10, 11, 12, 13, 14, 17, and 21. They were deeply anesthetized with 4% chloral hydrate (1 ml/100 g intraperitoneal, Fisher Scientific, Fair Lawn, NJ) and perfused through the aorta with 4% paraformaldehyde-4% sucrose in 0.1 M sodium phosphate buffered saline (PBS), pH 7.4. Brain stems were then removed, postfixed in the same fixative for 3 hours at 4°C, cryoprotected by immersion in increasing concentrations of sucrose (10, 20, and 30%) in 0.1 M PBS at 4°C, then frozen on dry ice and stored at −80°C until use.

Characterization of antibodies

Table 1 includes a brief summary of the antibodies used in the present study. Both antibodies (anti-BDNF and anti-TrkB) have been well characterized and their specificities established by the manufacturer and previous investigators. The anti-BDNF polyclonal antibody (sc-546, N-20; Santa Cruz Biotechnology, Santa Cruz, CA) was a purified immunoglobulin raised against an internal region of human BDNF and did not crossreact with neurotrophic factor 3 (NT-3) or nerve growth factor (NGF). By western blot analysis, this antibody specifically yielded a single band at ~14 kDa (Ricci et al., 2004) and did not show any immune signals in brain tissues of BDNF knockout mice (Tongiorgi et al., 2004). The immunoreactivity was abolished with preadsorption of this antibody (Ricci et al., 2004; Tongiorgi et al., 2004). This sc-546 pAb has been used by a number of investigative groups (e.g., Ricci et al., 2004; Tongiorgi et al., 2004; Hwang et al., 2005; Tan and Shepherd, 2006; Galvão et al., 2008; Matsumoto et al., 2008). The anti-TrkB rabbit polyclonal antibody (sc-12, Santa Cruz Biotechnology) was a purified immunoglobulin raised against the intracellular C-terminus (amino acid 794–808) of mouse TrkB and did not crossreact with tropomyosin-related kinase A or C (TrkA or TrkC). Its specificity was confirmed by a single band at the expected molecular size (~145 kDa) in western blots (Ricci et al., 2004; manufacturer's datasheet) and in preadsorption tests (Ricci et al., 2004). This antibody has also been used by several groups (including Ricci et al., 2004; Hecht et al., 2005; Lee et al., 2007).

Immunohistochemistry

Coronal sections (12- μm thickness) of frozen brain stems were cut with a Leica CM1900 cryostat (Leica Microsystems, Heidelberg, Nussloch, Germany). Seven sets of serial sections were mounted on gelatin-coated slides. In the same litter, sections from 3 (or 4) rats at different ages were mounted on the same slides and processed together. Ages were grouped typically as follows: P2-10-21, P0-3-4-17, P5-7-14, and P11-12-13. All sections from all rats were processed under identical conditions (i.e., time, temperature, and concentration of reagents). They were blocked overnight at 4°C with 5% nonfat dry milk-5% normal goat serum-1% Triton X-100 in 0.1 M PBS (pH 7.4). Sections were then incubated at 4°C for 36 hours in the primary antibodies diluted at the proper concentration in the same solution as used for blocking: 1:100 for rabbit anti-BDNF or 1:1,000 for rabbit anti-TrkB receptors. Sections were rinsed 3 times, 5 minutes each, in PBS, then incubated in the secondary antibodies: 1:100 goat antirabbit IgG-HRP (Bio-Rad, Hercules, CA), diluted in the modified blocking solution (without Triton X-100) for 4 hours at room temperature. After rinsing twice with PBS and once with 0.1 M ammonium phosphate buffer (APB), pH 7.0, immunoreactivity was detected with 0.05% DAB-0.004% H_2O_2 in APB for 5 minutes. The reaction was then stopped with APB for 5 minutes, rinsed in PBS three times, dehydrated, and coverslipped. Control sections were processed without primary antibodies or with a nonimmune serum in place of the primary antibodies.

One set of alternate sections was reacted for neurokinin-1 receptors using protocols described previously (Liu and Wong-Riley, 2002).

Semiquantitative optical densitometry

The immunoreactivity of BDNF and TrkB receptors in the cell bodies of individual neurons in various nuclei was semiquantitatively analyzed by optical densitometry performed with a Zeiss Zonax MPM 03 photometer, a 25 × objective, and a 2- μm-diameter measuring spot. White (tungsten) light was used for illumination, and all lighting conditions were held constant for all of the measurements. Since light intensity can directly affect optical densitometric values, a stepped density filter (Edmund Industrial Optics, Barrington, NJ) with 10-step increments of 0.1 (from 0.1 to 1) was used to precisely adjust the intensity of the light source to a standard value identical for all samples.

The boundary of each brain stem nucleus studied was determined with the aid of Paxinos and Watson's "The Rat Brain Atlas" (New York: Academic Press, 1986). The PBC was identified with the neurokinin-1 receptor labeling (Gray et al., 1999), its location according to the detailed descriptions of Smith et al. (1991), and as described in our previous articles (Liu and Wong-Riley, 2002, 2003, 2005). The part of the nucleus ambiguus chosen for the present study (and our previous studies: Liu and Wong-Riley, 2003, 2005, 2008) was the semicompact formation and the rostral loose formation innervating upper airway muscles with pharyngolaryngomotor functions (Bieger and Hopkins, 1987). The RTN was originally identified by Smith et al. (1989). The pFRG was described in the neonate with electrophysiological recordings and is located in the rostral ventrolateral medulla, ventrolateral to the facial nucleus and close to the ventral surface (Onimaru and Homma, 2003), apparently overlapping with the RTN (Feldman and Del Negro, 2006). Since it is not known if the RTN and pFRG are anatomically and functionally distinct (Feldman and Del Negro, 2006), we and others have opted to refer to this region as "RTN/pFRG." For the remaining nuclei, measurements were taken from the central main portion of each nucleus.

The optical densitometric value of each labeled neuron in the various brain stem nuclei studied was an average reading of two to four spots on the cell body (excluding the nucleus). Only those neurons whose nuclei were clearly visible (i.e., sectioned through the middle of the cell body) were measured. To avoid measuring the same neuron more than once, values were taken from cells in sections at least 84 μm apart, as the largest neurons had a maximal diameter of 25–30 μm, with a maximal nuclear diameter of only about 10 μm. About 100 neurons in each brain stem nucleus were measured for each marker in each rat, and a total of about 700 (for BDNF) or 1,100 (for TrkB receptor) at each age for each marker were measured. For statistical analyses, each sample's optical density value for each nucleus of each rat was the average of about 100 labeled neurons. Thus, the sample number at each timepoint in each nucleus for each marker was seven in Figure 6 and 11 in Figure 11. A total of 184,000 neurons were measured for the present study. Mean optical density values, standard deviations, and standard errors of the mean in each nucleus at each age were then obtained. Statistical comparisons were made among the age groups using one-way analysis of variance (ANOVA) (to control for the type I comparison-wise error rate) and, when significant differences were found, comparisons were made between successive age groups (e.g., P2 vs. P3, P3 vs. P4, and P5 vs. P7) using Tukey's Studentized range test (post-hoc multiple comparisons, to control for the type I experiment-wise error rate). Additional Tukey's tests were conducted between two groups that were not immediately adjacent to each other, and significant differences, if any, are presented in the Results section (but not shown in the graphs to minimize confusion). Significance was set at $P < 0.01$ for one-way ANOVA and $P < 0.05$ for Tukey's test.

The photomicrographs were taken with the CCD camera (SPOT RT3) mounted on a light microscope (Nikon E600) using SPOT Advanced 4.6 software (Diagnostic Instruments, Sterling Heights, MI) and processed with Adobe Photoshop 6.0 (San Jose, CA). Contrast and brightness adjustments were identical for all photomicrographs in each plate.

RESULTS

BDNF-immunoreactive neurons in multiple brain stem nuclei

BDNF immunoreactivity (-ir) was clearly visible in subpopulations of neurons in all brain stem nuclei examined (Figs. 1A–E, 2–5). Immunoreaction product was present in cell bodies and proximal dendrites of labeled neurons and in dendrites and axons of the neuropil. In addition to the cytoplasm, the plasma membrane of many labeled neurons also exhibited immunoreaction product (see insets in Figs. 2–5). Nuclear labeling was more common in younger animals before P10, but was also present in some neurons in older animals (Figs. 2–5), in agreement with previous reports of nuclear labeling in other parts of the rat brain, where BDNF is thought to influence transcription (Wet-more et al., 1991; Nitta et al., 1997; Furukawa et al., 1998). The sizes of BDNF-ir neurons increased with age and reached a relatively stable level around P11 (Figs. 2–5). Control sections had no specific immunoreactivity above background (data not shown). ANOVA indicated significant differences ($P < 0.01$) in optical densitometric values of individual BDNF-ir neurons among the ages in all eight nuclei examined. Tukey's Studentized range test that compared one age group with its adjacent younger age group revealed significant differences in the intensity of BDNF-ir between two adjacent age groups in specific nuclei described below and shown in graphs for each nucleus (Fig. 6; significance marked by asterisks). Additional Tukey's comparisons between nonadjacent age groups are indicated in the text below but not shown in the graphs.

BDNF-immunoreactivity in the PBC

BDNF-ir was observed in ~50–75% of the PBC neurons. They were multipolar, granular, or fusiform in shape and small and medium in size (Fig. 2A–D). The size of small neurons ranged from 4.5–7.5 μm in diameter at P2 to 7.5–11 μm at P21, and medium-sized neurons ranged from 10–13 μm at P2 to 15–21 μm at P21. Among labeled neurons, 30–45% showed immunoreaction product along the plasma membrane (see inset in Fig. 2A). Approximately 45–55% in the P0 to P7 age groups had nuclear labeling, and this percentage dropped to ~15–25% in the P10 to P21 age groups. The neuropil was light to moderately immunoreactive, with a punctate distribution during the third postnatal week. Optical densitometric analysis of individual labeled neurons indicated that the expression of BDNF was relatively high from P0 to 11, but decreased significantly at P12 ($P < 0.01$) and remained low at P13, followed by a significant rise at P14 ($P < 0.05$) and a gradual decline until P21 (Fig. 6A). Additional Tukey's test revealed that the value at P21 was significantly lower than those of individual days from P0 to P11 as well as of P14 ($P < 0.05$ – $P < 0.001$; significance not shown in Fig. 6A).

BDNF-immunoreactivity in the Amb

About 55–85% of Amb neurons demonstrated BDNF-ir. They were multipolar or oval in shape and mainly medium or small in size (Fig. 2E–H). The size of small neurons ranged from 6.5 to 8 lm in diameter at P2 to 9–12 μm at P21, and medium-sized neurons ranged from 10–13.5 μm at P2 to 17–23.5 μm at P21. Approximately 30–40% of labeled neurons had immunoreactivity along the plasma membrane (see insets in Fig. 2F). About 40–60% of labeled neurons at P0 to P13 and only ~15% at P21 showed nuclear labeling. The neuropil was light to moderately immunoreactive before P10, but the labeling increased to moderate with a punctate appearance in P10–21 animals. BDNF-ir as measured by optical

densitometry was at a relatively high level from P0 to P11, but was significantly reduced at P12 ($P < 0.001$), followed by a gradual increase at P13 and P14, before plateauing until P21 (Fig. 6B). Additional Tukey's tests revealed a significant difference between P12 and P14 ($P < 0.01$)

BDNF-immunoreactivity in the NTS_{VL}

BDNF-ir was present in about 55–80% of the NTS_{VL} neurons. They were multipolar, granular, or oval in shape and mainly small in size (Fig. 3A–D). The small neurons ranged from 4.5–8.5 μm in diameter at P2 to 6.5–13 μm at P21. Plasma membrane immunoreactivity was observed in about 25–35% of labeled neurons (see inset in Fig. 3A). Approximately 20–35% of labeled neurons exhibited nuclear labeling in P0 to P13 rats, but only about 10% in P21 animals. The intensity of labeling in the neuropil was light to moderate during the first week, but increased progressively in the second and third weeks. The expression of BDNF analyzed by optical densitometry was relatively high from P0 to P11, but fell significantly at P12 ($P < 0.01$), followed by a rise and a plateau until P21 (Fig. 6C).

BDNF-immunoreactivity in the NTS_{COM}

BDNF-ir was observed in ~50–75% of neurons in the NTS_{COM}. They were small in size and multipolar, oval, or granular in shape (Fig. 3E–H). The size ranged from 4.5–8 μm in diameter at P2 to 6–12 μm at P21. About 15–30% of labeled neurons showed distinct plasma membrane labeling (see inset in Fig. 3E), and 30–40% had nuclear labeling. The neuropil was moderate to lightly immunoreactive. The expression of BDNF exhibited a significant rise from P0 to P2 ($P < 0.05$) followed by a plateau until P11, then a significant fall at P12 ($P < 0.01$) followed by a marked increase at P13 ($P < 0.01$) and plateaued thereafter until P21 (Fig. 6D).

BDNF-immunoreactivity in the RTN/pFRG

Approximately 30–50% of the RTN/pFRG neurons were BDNF-ir. They were multipolar, granular, or fusiform in shape and small or medium in size (Fig. 4A–D). About 30–40% of labeled neurons at P0–13 and only ~10% at P21 exhibited nuclear labeling, and ~30–60% of labeled neurons had detectable plasma membrane labeling (see inset in Fig. 4C). The neuropil was moderate to lightly labeled. The developmental trend of BDNF-ir was relatively constant from P0 to P21, except for a significant fall at P12 ($P < 0.05$) (Fig. 6E).

BDNF-immunoreactivity in the LPGi

About 30–40% of neurons in the LPGi exhibited BDNF-ir. They were mainly multipolar or fusiform in shape, small or medium in size, with medium ones appearing around P11 and thereafter (Fig. 4E–H). Small neurons ranged from 4 to 9 μm in diameter at P2 to 5–11 μm at P21, and the medium-sized ones ranged from 13.5–18 μm in diameter at P11–21. Approximately 30–50% of labeled neurons exhibited plasma membrane immunoreactivity (see inset in Fig. 4F), and about 30–55% had nuclear labeling. The neuropil was light to moderately immunoreactive. Optical densitometric analysis indicated that BDNF-ir was relatively low at P0, rose slightly from P2 to P4 but significantly at P7 ($P < 0.01$), followed by a striking reduction at P10 ($P < 0.01$) and a plateau thereafter until P21 (Fig. 6F). Additional Tukey's tests showed that BDNF level at P7 was significantly higher than those of other days examined during the first 3 postnatal weeks ($P < 0.01$ – $P < 0.001$).

BDNF-immunoreactivity in the pPy

Approximately 35–45% of pPy neurons were BDNF-ir, and they were small or medium in size (with medium ones appearing around P11 and thereafter) and multipolar, fusiform, or

granular in shape (Fig. 5A–D). Small neurons ranged from 3.5–8.5 μm in diameter at P2 to 4.5–11.5 μm at P21, and medium-sized neurons ranged from 13–18.5 μm in diameter at P11–21. About 40–50% of labeled neurons at P0 to P13 showed plasma membrane immunoreactivity, but this percentage dropped to ~25% at P21 (see inset in Fig. 5C). Approximately 30–50% of labeled neurons exhibited nuclear labeling. The neuropil was light to moderately immunoreactive. BDNF-ir as measured by optical densitometry increased gradually from P0 to P7, but was significantly reduced at P10 ($P < 0.01$), followed by a statistically insignificant rise at P11 and a plateau thereafter until P21 (Fig. 6G). Tukey's test also revealed that the BDNF-ir level at P7 was significantly higher than those at P0, P17, and P21 ($P < 0.05$ – $P < 0.01$).

BDNF-immunoreactivity in the CN

About 30–50% of neurons in the CN demonstrated BDNF-ir (Fig. 5E–H). They were oval, multipolar, or granular in shape and mainly small in size, with a few mediumsized ones. Small neurons ranged from 4–7 μm in diameter at P2 to 6.5–11 μm at P21, and medium-sized ones ranged from 8.5–11 μm at P2 to 12.5–15 μm at P21. Approximately 15–40% of labeled neurons showed plasma membrane immunoreactivity (see inset in Fig. 5F), whereas nuclear labeling was found in about 10–40% of them. The intensity of neuropil immunoreactivity rose from P11 to P21, with punctate or globular distribution (Fig. 5E–H). The expression of BDNF as measured with optical densitometry was relatively high from P0 to P11, followed by a gradual decrease with age until P21 (Fig. 6H). There were no significant differences between any two adjacent age groups, but Tukey's test did indicate that the values at P17 and P21 were significantly lower than those of individual days from P0 to P12 ($P < 0.01$ – $P < 0.001$), and the value at P21 was lower than those at P13 and P14 ($P < 0.01$).

TrkB-immunoreactive neurons in multiple brain stem nuclei

TrkB-ir was clearly visible in subpopulations of neurons in each of the brain stem nuclei examined (Figs. 1F–J, 7–10). Labeling was present in cell bodies and proximal dendrites of neurons as well as in dendrites and axons of the neuropil. There was no nuclear labeling. In addition to the cytoplasm, the plasma membrane of many labeled neurons showed clear immunoreaction product (see insets in Figs. 7–10), but the intensity decreased somewhat at P21. At P0 to P10, labeling in the cytoplasm was relatively homogeneous, but around P11–12 and later it became more punctate or granular, especially in the PBC, Amb, and LPGi (arrowheads in Figs. 7D,7H, 9H). Some glial cells, much smaller in size than neurons, exhibited TrkB-ir around P11 and later. Glial cells were not included in our optical densitometric analyses. The sizes, shapes, developmental trends, and prevalence of TrkB-ir neurons were comparable to those of BDNF-ir neurons, and will not be described in detail below. Control sections demonstrated no specific immunoreactive product above background (data not shown). ANOVA indicated significant differences ($P < 0.01$) in TrkB-ir among the ages in all eight nuclei examined. Tukey's tests revealed significant differences in the intensity of TrkB-ir between two adjacent age groups in specific nuclei described below and shown in graphs for each nucleus (Fig. 11; significance marked by asterisks). Additional Tukey's comparisons between nonadjacent age groups are indicated in the text below but not shown in the graphs.

TrkB-immunoreactivity in the PBC

TrkB-ir was visible in ~50–75% of neurons in the PBC (Fig. 7A–D), and about 30–50% of them showed plasma membrane labeling (see inset in Fig. 7A). At P0 to P10, immunoreaction product appeared relatively homogeneous in the cytoplasm, but it became more punctate and granular afterwards, with ~90% of neurons at P21 possessing that pattern (arrowheads in Fig. 7D). TrkB-ir as measured by optical densitometry in individual neurons

was the lowest at P0–2, increased gradually to peak at P10, then fell significantly at P12 ($P < 0.01$). It remained low at P13, but rose significantly at P14 ($P < 0.01$) and fell again until P21 (Fig. 11A). Additional Tukey's tests revealed that the values at P10 and P14 were significantly higher than those at P0, P2, and P12 ($P < 0.05 – P < 0.001$), and P10 and P11 values were significantly higher than that at P13 ($P < 0.001$ or $P < 0.05$, respectively).

TrkB-immunoreactivity in the Amb

Approximately 60–80% of neurons in the Amb exhibited TrkB-ir (Fig. 7E–H), and among them, 20–45% had clearly resolvable immunoreaction product along the plasma membrane (see inset in Fig. 7F). The developmental pattern of TrkB-ir in the cytoplasm was similar to that in the PBC, with more homogeneous distribution before P10, and more granular ones afterwards until P21 (arrowheads in Fig. 7H). The intensity of TrkB-ir in individual neurons was relatively constant from P0 to P21, except for a significant reduction at P12 and P13 that differed from all of the other timepoints ($P < 0.05 – P < 0.001$) (Fig. 11B).

TrkB-immunoreactivity in the NTS_{VL}

TrkB-ir was detected in about 40–65% of neurons in the NTS_{VL} (Fig. 8A–D), and ~25–40% of them had well-defined plasma membrane labeling (see inset in Fig. 8A). TrkB-ir was homogeneously distributed in the cytoplasm of almost 100% of labeled neurons at P0, ~50% of neurons from P2 to P17, and 75% at P21 (Fig. 8A–D). The remaining ones exhibited more granular labeling in the cytoplasm. The intensity of TrkB-ir was the lowest at P0–2, increased significantly at P3 ($P < 0.01$), and rose again gradually until P11. It then fell considerably at P12 ($P < 0.001$), followed by a gradual increase until P21 (Fig. 11C). Additional Tukey's tests yielded significant differences between P11 and individual days between P0 and P5 ($P < 0.05 – P < 0.001$), between P12 and 17 ($P < 0.05$) or P21 ($P < 0.01$), as well as between P0 or P2 and individual days at P14, P17, and P21 ($P < 0.001$ for all).

TrkB-immunoreactivity in the NTS_{COM}

Approximately 55–85% of NTS_{COM} neurons were TrkB-ir (Fig. 8E–H), and about 20–50% of labeled neurons showed distinct plasma membrane labeling (see inset in Fig. 8F). Labeling was homogeneous in almost 100% of labeled neurons during the first week, ~70% of neurons in the second week, and ~30% at P21, whereas the remaining ones were more punctate (Fig. 8E–H). The expression of TrkB increased with age from P0 to P21, except for a significant fall at P12 ($P < 0.05$) followed by a marked rise at P13 ($P < 0.05$) to a level comparable to that at P11 (Fig. 11D). Additional Tukey's tests revealed that the expression level at P0, P2, or P3 was significantly lower than that at P21 ($P < 0.05 – P < 0.01$). The level at P2 was also significantly lower than that at P17 ($P < 0.05$), and the level at P14, P17, or P21 was significantly high than that at P12 ($P < 0.05 – P < 0.01$).

TrkB-immunoreactivity in the RTN/pFRG

About 25–40% of RTN/pFRG neurons exhibited TrkB-ir (Fig. 9A–D) and ~25–45% of labeled neurons showed distinct plasma membrane labeling (see inset in Fig. 9B). The labeling in the cytoplasm was predominantly homogeneous from P0 to P10, but ~50% of labeled neurons exhibited a more granular pattern thereafter (Fig. 9A–D). The expression of TrkB increased from P0 to P11, then fell significantly at P12 ($P < 0.01$), followed by a significant rise at P13 ($P < 0.01$) and plateaued thereafter until P21 (Fig. 11E). Additional Tukey's tests revealed that the expression at individual day from P0 to P5 was significantly lower than those at P14, P17, or P21 ($P < 0.01 – P < 0.001$), and the expression at P12 was also significantly lower than those at P10, P14, or P21.

TrkB-immunoreactivity in the LPGi

TrkB-ir was visible in about 35–50% of LPGi neurons (Fig. 9E–H), and plasma membrane labeling was observed in ~ 30–65% of them (see inset in Fig. 9F). TrkB-ir distribution in the cytoplasm changed from predominantly homogeneous to more granular with age (Fig. 9E–H, and arrowheads in 9H) just as it did in the PBC and Amb. The intensity of TrkB-ir followed a trend similar to that of BDNF, with the lowest value at P0, a significant increase at P7 ($P < 0.01$), and a striking reduction at P10 ($P < 0.01$), followed by a plateau thereafter until P21 (Fig. 11F). Additional Tukey's comparisons yielded significant differences between P7 and individual days from P0 to P21 ($P < 0.05 – P < 0.001$), and between P10 and P0 or P2 ($P < 0.05$ for both).

TrkB-immunoreactivity in the pPy

Approximately 40–55% of pPy neurons demonstrated TrkB-ir (Fig. 10A–D), and among them ~40–55% had demonstrable plasma membrane labeling (see inset in Fig. 10B). The majority of neurons at all age groups had relatively homogeneous labeling in their cytoplasm, with a small percentage of them exhibiting small granular labeling. TrkB-ir as measured by optical densitometry in individual neurons was low at P0–2, increased gradually to reach a peak at P7, followed by a significant fall at P10 ($P < 0.05$), and plateaued thereafter until P21 (Fig. 11G). Tukey's tests also revealed that values at P0 and P2 were significantly lower than those at P5, P7, and P12 to P17 ($P < 0.05 – P < 0.001$), whereas that at P7 was significantly higher than those at P3, P4, and P11 ($P < 0.05 – P < 0.01$).

TrkB-immunoreactivity in the CN

About 40–60% of neurons in the CN exhibited TrkB-ir (Fig. 10E–H), and ~25–40% of them showed plasma membrane labeling (see inset in Fig. 10E). The majority of immunoreaction product was distributed rather evenly in the cytoplasm, although in older animals (after P10) it became more granular and punctate. The intensity of TrkB-ir was relatively low at P0 and P2, but rose to a small peak at P10, followed by a plateau until P21 (Fig. 11H). Although there were no significant day-to-day differences, Tukey's tests did reveal that the values at P0 and P2 were significantly lower than those at individual days between P10 and P21 ($P < 0.05 – P < 0.001$).

DISCUSSION

The present large-scale, in-depth, developmental study of the first 3 postnatal weeks revealed for the first time that a significant reduction in the expressions of both BDNF and TrkB occurred at P12 in the PBC, Amb, NTS_{VL}, NTS_{COM}, and RTN/pFRG, whereas that in the LPGi and pPy occurred at P10. Such reductions were not found in the nonrespiratory cuneate nucleus.

Technical considerations

The validity of immunohistochemistry is dependent mainly on the specificity of the antibody and is a reflection of relative protein amount. The antibodies used in the current study were polyclonal ones and were well documented for their specificity (see Materials and Methods). Our approach has the distinct advantage of localizing relative protein expressions in individual neurons rather than in mixed populations of neurons, glia, and endothelial cells as in immunoblots. The large number of animals used, the close timepoints of postnatal ages examined, and the 184,000 individual neurons measured all enhanced our confidence in the statistical significance of the present findings.

Developmental trends of BDNF and TrkB

The expressions of BDNF and TrkB themselves are known to be developmentally regulated. However, only a few postnatal timepoints were examined in previous studies. In general, BDNF-ir is low at birth and increases with age, with either a plateau or a decline in the adult (Katoh-Semba et al., 1997; Das et al., 2001; Kim et al., 2007). There appears to be a caudorostral progression of development, as BDNF mRNA is already detectable in the rat spinal cord at embryonic days 12 and 13 and the level peaks at birth (Maisonpierre et al., 1990), but the levels of both BDNF message and protein are low in the rat neo-cortex and hippocampus in the neonate and do not peak until P14–20 (Katoh-Semba et al., 1997; Das et al., 2001). The clear presence of BDNF-ir at birth and its general peak around P7–11 in all eight nuclei examined in the present study indicate that BDNF development in the brain stem is between those of the spinal cord and higher centers. This agrees with findings in the rat inferior olivary complex, where BDNF expression is relatively high during the first week (Rocamora et al., 1993).

The development of TrkB-ir appears to lag slightly behind that of BDNF, as the levels in all eight nuclei in the present study were low at P0–2, and rose progressively to peak at P10–11 (although earlier at P7 in LPGi and pPy). The level at P21 was, in general, much higher than that in the newborn (except for PBC and Amb, where the levels were comparable to those of the neonate). Slight variations in the developmental trend of TrkB were also noted in other brain stem nuclei (Hafidi et al., 1996; Riva-Depaty et al., 1998).

BDNF and TrkB play an important role in the development of brain stem neurons involved in respiratory control and the expression of normal breathing after birth (Erickson et al., 1996; Balkowiec and Katz, 1998; Katz, 2005; Katz et al., 2009; Kline et al., 2010). This is verified by the prevalence of BDNF and TrkB in multiple respiratory-related nuclei during the first 3 postnatal weeks (the present study). BDNF knockout animals lack a subset of afferents involved in ventilatory control and demonstrate a severe respiratory disorder (Erickson et al., 1996). Exogenous BDNF or TrkB agonist can restore breathing disorder induced by BDNF knockout or deficit (Kline et al., 2010; Schmid et al., 2012). BDNF is also essential for respiratory plasticity (Baker-Herman et al., 2004).

Critical period of respiratory development

The most striking finding of the present study is the abrupt and statistically significant fall in the expressions of both BDNF and TrkB during the critical period of respiratory development in multiple brain stem respiratory-related nuclei but not in the nonrespiratory cuneate nucleus. The fall at P12 in the PBC, Amb, and NTS_{VL} coincides precisely in time with a sudden and statistically significant decrease in the expressions of excitatory neurochemicals (glutamate and N-methyl-$_D$-aspartate [NMDA] receptor subunits 1 and 2A) and a sudden and significant rise in the expressions of inhibitory neuro-chemicals (GABA, $GABA_B$, and glycine receptors) in these same nuclei (Liu and Wong-Riley, 2002, 2004, 2006, 2008, 2010c). Moreover, a heightened inhibition and suppressed excitation is demonstrable electrophysiologically in hypoglossal neurons at P12 and P13 (Gao et al., 2011). The link between the neurochemical imbalance and a reduction in BDNF-TrkB is 3-fold: 1) As discussed above, BDNF-TrkB are essential in the development of the respiratory system; 2) BDNF is found to enhance excitatory neurotransmission and to suppress inhibitory ones (Wardle and Poo, 2003). The facilitation of glutamatergic synaptic transmission is via both pre- and postsynaptic mechanisms (Small et al., 1998; Narisawa-Saito et al., 1999; Schinder et al., 2000; Caldeira et al., 2007a,b; Carvalho et al., 2008; Balu and Coyle, 2011; Martin and Finsterwald, 2011; Kim et al., 2012), as is the depression of GABAergic transmission (Frerking et al., 1998; Wardle and Poo, 2003; Jovanovic et al., 2004; Kron et al., 2007; Lund et al., 2008). BDNF reduces the frequency of spontaneous

IPSC (sIPSC) and the amplitude of evoked IPSC (eIPSC) in the Kölliker-Fuse nucleus of postnatal rats (Kron et al., 2007). The effect of BDNF on GABAergic and/or glycinergic transmission may in part be mediated through its modulation of the Cl^- exporter K^+–Cl^- cotransporter 2 (KCC2) (Rivera et al., 2002, 2004; Mizoguchi et al., 2003; Fiumelli and Woodin, 2007), which reportedly varies with development (Aguado et al., 2003; Rivera et al., 2002, 2004; Ludwig et al., 2011); and 3) Whereas BDNF regulates the release of glutamate and expressions of NMDA, non-NMDA, and GABA receptors (Small et al., 1998; Narisawa-Saito et al., 1999; Caldeira et al., 2007a,b; Lund et al., 2008; Kim et al., 2012), BDNF itself is regulated by NMDAR, non-NMDAR, and GABAergic receptors (Thoenen et al., 1991; Berninger et al., 1995; Xiong et al., 2002; Marmigère et al., 2003; Garoflos et al., 2005; Khundakar and Zetterström, 2011). Thus, during the critical period the downregulation of BDNF-TrkB would initially weaken their facilitatory influence on excitatory neurochemicals and suppressive influence on inhibitory neurochemicals, leading to the observed neuro-chemical imbalance. In turn, however, the affected neuro-chemicals will alter their impact on BDNF-TrkB, thus reinforcing the imbalance at that time.

BDNF is also known to play an important role in serotonin synthesis and in maintaining the postsynaptic serotonin 5-HT_{2A} receptors (Eaton et al., 1995; Rios et al., 2006). In turn, BDNF is regulated by 5-HT_{1A} and 5-$HT_{2A/C}$ receptor-mediated mechanisms (Garoflos et al., 2005). Indeed, BDNF and serotonin are found to mutually enhance each other's expression (Martinowich and Lu, 2008). Significantly, the downregulation of BDNF-TrkB at P12 in the PBC, Amb, NTS_{VL}, NTS_{COM}, RTN/pFRG (present study) is matched precisely by a precipitous fall in the expressions of serotonin transporter (SERT), 5-HT_{1A}, 5-HT_{1B}, and 5-HT_{2A} receptors in these same nuclei at the same time (Liu and Wong-Riley, 2008, 2010a,b). Moreover, the downregulation of BDNF-TrkB at P10 in the LPGi and pPy (present study) corresponds in time to a significant fall in the expression of SERT in these same nuclei (Liu and Wong-Riley, 2010b). The earlier onset of change in the LPGi and pPy strongly suggests that they exert a more global and inductive role on the other brain stem respiratory-related nuclei, especially when they have a widespread projection to the ventral and dorsal respiratory groups (Zec and Kinney, 2001; Cream et al., 2002; Van Bockstaele et al., 2004; Ribas-Salgueiro et al., 2005). Thus, BDNF and TrkB are likely to regulate the expressions of serotoninergic neurochemicals, which, in turn, exert their feedback modulation onto BDNF and TrkB.

The temporal and spatial coincidence of a downregulation of BDNF/TrkB and these neurochemicals strongly supports our hypothesis that BDNF/TrkB plays an important role in mediating the excitatory-inhibitory imbalance within the respiratory network during the critical period of postnatal development in the rat. Moreover, both BDNF and serotonin are important regulators of development and plasticity, and their concomitant and significant downregulation in the same respiratory-related nuclei at the same time further emphasizes the functional significance of the critical period. A downregulation of BDNF/ TrkB expressions in the PBC, Amb, NTS_{VL}, NTS_{COM}, and RTN/pFRG at P12 would negatively affect respiratory rhythmogenesis, upper airway patency, and chemosensitivity. It would also attenuate the hypoxic respiratory response, which was precisely what we found at P12–13, when the response to hypoxia was the weakest as compared to other timepoints during the entire first 3 postnatal weeks in the rat (Liu et al., 2006).

In sum, BDNF and its receptor TrkB are likely to exert an important neurotrophic influence on the development of multiple respiratory-related nuclei in the brain stem. Their sudden downregulation in these nuclei during the critical period may form the basis of, or at least contribute to, the striking set of neurochemical, ventilatory, and electrophysiological changes observed at that time (Wong-Riley and Liu, 2005, 2008; Liu et al., 2006, 2008; Liu and Wong-Riley, 2010a–c; Gao et al., 2011).

Acknowledgments

Grant sponsor: National Institutes of Health; Grant number: R01 HD048954.

LITERATURE CITED

Aguado F, Carmona MA, Pozas E, Aguiló A, Martínez-Guijarro FJ, Alcantara S, Borrell V, Yuste R, Ibañez CF, Soriano E. BDNF regulates spontaneous correlated activity at early developmental stages by increasing synaptogenesis and expression of the K+/Cl− co-transporter KCC2. Development. 2003; 130:1267–1280. [PubMed: 12588844]

Baker-Herman TL, Fuller DD, Bavis RW, Zabka AG, Golder FJ, Doperalski NJ, Johnson RA, Watters JJ, Mitchell GS. BDNF is necessary and sufficient for spinal respiratory plasticity following intermittent hypoxia. Nat Neurosci. 2004; 7:48–55. [PubMed: 14699417]

Balkowiec A, Katz DM. Brain-derived neurotrophic factor is required for normal development of the central respiratory rhythm in mice. J Physiol. 1998; 510:527–533. [PubMed: 9706001]

Balu DT, Coyle JT. Neuroplasticity signaling pathways linked to the pathophysiology of schizophrenia. Neurosci Biobehav Rev. 2011; 35:848–870. [PubMed: 20951727]

Bardoni R, Ghirri A, Salio C, Prandini M, Merighi A. BDNF-mediated modulation of GABA and glycine release in dorsal horn lamina II from postnatal rats. Dev Neurobiol. 2007; 67:960–975. [PubMed: 17506495]

Bartkowska K, Turlejski K, Djavadian RL. Neurotrophins and their receptors in early development of the mammalian nervous system. Acta Neurobiol Exp (Wars). 2010; 70:454–467. [PubMed: 21196952]

Berninger B, Marty S, Zafra F, da Penha Berzaghi M, Thoenen H, Lindholm D. GABAergic stimulation switches from enhancing to repressing BDNF expression in rat hippocampal neurons during maturation in vitro. Development. 1995; 121:2327–2335. [PubMed: 7671799]

Bieger D, Hopkins DA. Viscerotopic representation of the upper alimentary tract in the medulla oblongata in the rat: the nucleus ambiguus. J Comp Neurol. 1987; 262:546–562. [PubMed: 3667964]

Bonham AC. Neurotransmitters in the CNS control of breathing. Respir Physiol. 1995; 101:219–230. [PubMed: 8606995]

Caldeira MV, Melo CV, Pereira DB, Carvalho R, Correia SS, Backos DS, Carvalho AL, Esteban JA, Duarte CB. Brain-derived neurotrophic factor regulates the expression and synaptic delivery of alpha-amino-3-hydroxy-5-methyl-4-isoxazole propionic acid receptor subunits in hippocampal neurons. J Biol Chem. 2007a; 282:12619–12628. [PubMed: 17337442]

Caldeira MV, Melo CV, Pereira DB, Carvalho RF, Carvalho AL, Duarte CB. BDNF regulates the expression and traffic of NMDA receptors in cultured hippocampal neurons. Mol Cell Neurosci. 2007b; 35:208–219. [PubMed: 17428676]

Carvalho AL, Caldeira MV, Santos SD, Duarte CB. Role of the brain-derived neurotrophic factor at glutamatergic synapses. Br J Pharmacol. 2008; 153(Suppl 1):S310–324. [PubMed: 18059328]

Cream C, Li A, Nattie E. The retrotrapezoid nucleus (RTN): local cytoarchitecture and afferent connections. Respir Physiol Neurobiol. 2002; 130:121–137. [PubMed: 12380003]

Das KP, Chao SL, White LD, Haines WT, Harry GJ, Tilson HA, Barone S Jr. Differential patterns of nerve growth factor, brain-derived neurotrophic factor and neurotrophin-3 mRNA and protein levels in developing regions of rat brain. Neuroscience. 2001; 103:739–761. [PubMed: 11274792]

Eaton MJ, Staley JK, Globus MY, Whittemore SR. Developmental regulation of early serotonergic neuronal differentiation: the role of brain-derived neurotrophic factor and membrane depolarization. Dev Biol. 1995; 170:169–182. [PubMed: 7601307]

Erickson JT, Conover JC, Borday V, Champagnat J, Barbacid M, Yancopoulos G, Katz DM. Mice lacking brain-derived neurotrophic factor exhibit visceral sensory neuron losses distinct from mice lacking NT4 and display a severe developmental deficit in control of breathing. J Neurosci. 1996; 16:5361–5371. [PubMed: 8757249]

Feldman JL. Chapter 14—looking forward to breathing. Prog Brain Res. 2011; 188:213–218. [PubMed: 21333812]

Feldman JL, Del Negro CA. Looking for inspiration: new perspectives on respiratory rhythm. Nat Rev Neurosci. 2006; 7:232–242. [PubMed: 16495944]

Finley JCW, Katz DM. The central organization of carotid body afferent projection to the brain stem of the rat. Brain Res. 1992; 572:108–116. [PubMed: 1611506]

Fiumelli H, Woodin MA. Role of activity-dependent regulation of neuronal chloride homeostasis in development. Curr Opin Neurobiol. 2007; 17:81–86. [PubMed: 17234400]

Frerking M, Malenka RC, Nicoll RA. Brain-derived neurotrophic factor (BDNF) modulates inhibitory, but not excitatory, transmission in the CA1 region of the hippocampus. J Neurophysiol. 1998; 80:3383–3386. [PubMed: 9862938]

Furukawa S, Sugihara Y, Iwasaki F, Fukumitsu H, Nitta A, Nomoto H, Furukawa Y. Brain-derived neurotrophic factor-like immunoreactivity in the adult rat central nervous system predominantly distributed in neurons with substantial amounts of brain-derived neurotrophic factor messenger RNA or responsiveness to brain-derived neurotrophic factor. Neuroscience. 1998; 82:653–670. [PubMed: 9483526]

Galvão RP, Garcia-Verdugo JM, Alvarez-Buylla A. Brain-derived neurotrophic factor signaling does not stimulate subventricular zone neurogenesis in adult mice and rats. J Neurosci. 2008; 28:13368–13383. [PubMed: 19074010]

Gao XP, Liu QS, Liu Q, Wong-Riley MTT. Excitatory-inhibitory imbalance in hypoglossal neurons during the critical period of postnatal development in the rat. J Physiol. 2011; 589:1991–2006. [PubMed: 21486774]

Garoflos E, Stamatakis A, Mantelas A, Philippidis H, Stylianopoulou F. Cellular mechanisms underlying an effect of “early handling” on pCREB and BDNF in the neonatal rat hippocampus. Brain Res. 2005; 1052:187–195. [PubMed: 16024004]

Gray PA, Rekling JC, Bocchiaro CM, Feldman JL. Modulation of respiratory frequency by peptidergic input to rhythmogenic neurons in the pre-Bötzinger complex. Science. 1999; 286:1566–1568. [PubMed: 10567264]

Guyenet PG, Stornetta RL, Bayliss DA, Mulkey DK. Retrotrapezoid nucleus: a litmus test for the identification of central chemoreceptros. Exp Physiol. 2005; 90:247–257. [PubMed: 15728136]

Hafidi A, Moore T, Sanes DH. Regional distribution of neurotrophin receptors in the developing auditory brainstem. J Comp Neurol. 1996; 367:454–464. [PubMed: 8698904]

Hecht M, Schulte JH, Eggert A, Wilting J, Schweigerer L. The neurotrophin receptor TrkB cooperates with c-Met in enhancing neuroblastoma invasiveness. Carcinogen-esis. 2005; 26:2105–2115.

Hofer MM, Barde YA. Brain-derived neurotrophic factor prevents neuronal death in vivo. Nature. 1988; 331:261–262. [PubMed: 3336438]

Holtman JR Jr, Marion LJ, Speck DF. Origin of serotonin-containing projections to the ventral respiratory group in the rat. Neuroscience. 1990; 37:541–552. [PubMed: 2133358]

Hwang JJ, Park MH, Choi SY, Koh JY. Activation of the Trk signaling pathway by extracellular zinc. Role of metalloproteinases. J Biol Chem. 2005; 280:11995–12001.

Jordan D. Central nervous pathways and control of the airways. Respir Physiol. 2001; 125:67–81. [PubMed: 11240153]

Jovanovic JN, Thomas P, Kittler JT, Smart TG, Moss SJ. Brain-derived neurotrophic factor modulates fast synaptic inhibition by regulating GABA(A) receptor phosphorylation, activity, and cell-surface stability. J Neurosci. 2004; 24:522–530. [PubMed: 14724252]

Kaisho Y, Shintani A, Ono Y, Kato K, Igarashi K. Regional expression of the nerve growth factor gene family in rat brain during development. Biochem Biophys Res Commun. 1991; 174:379–385. [PubMed: 1989616]

Katoh-Semba R, Takeuchi IK, Semba R, Kato K. Distribution of brain-derived neurotrophic factor in rats and its changes with development in the brain. J Neurochem. 1997; 69:34–42. [PubMed: 9202291]

Katz DM. Regulation of respiratory neuron development by neurotrophic and transcriptional signaling mechanisms. Respir Physiol Neurobiol. 2005; 149:99–109. [PubMed: 16203214]

Katz DM, Dutschmann M, Ramirez JM, Hilaire G. Breathing disorders in Rett syndrome: progressive neurochemical dysfunction in the respiratory network after birth. Respir Physiol Neurobiol. 2009; 168:101–108. [PubMed: 19394452]

Khundakar AA, Zetterström TS. Effects of GABAB ligands alone and in combination with paroxetine on hippocampal BDNF gene expression. Eur J Pharmacol. 2011; 671:33–38. [PubMed: 21930121]

Kim JK, Jeon SM, Lee KM, Park ES, Cho HJ. Expression of brain-derived neurotrophic factor in the rat forebrain and upper brain stem during postnatal development: an immunohistochemical study. Neuroscience. 2007; 146:1128–1136. [PubMed: 17395388]

Kim JH, Roberts DS, Hu Y, Lau GC, Brooks-Kayal AR, Farb DH, Russek SJ. Brain-derived neurotrophic factor uses CREB and Egr3 to regulate NMDA receptor levels in cortical neurons. J Neurochem. 2012; 120:210–219. [PubMed: 22035109]

Kline DD, Ogier M, Kunze DL, Katz DM. Exogenous brain-derived neurotrophic factor rescues synaptic dysfunction in Mecp2-null mice. J Neurosci. 2010; 30:5303–5310. [PubMed: 20392952]

Kron M, Zhang W, Dutschmann M. Developmental changes in the BDNF-induced modulation of inhibitory synaptic transmission in the Kölliker-Fuse nucleus of rat. Eur J Neurosci. 2007; 26:3449–3457. [PubMed: 18052976]

Lee E, Jeong YI, Park SM, Lee JY, Kim JH, Park SW, Hossein MS, Jeong YW, Kim S, Hyun SH, Hwang WS. Beneficial effects of brain-derived neurotropic factor on *in vitro* maturation of porcine oocytes. Reproduction. 2007; 134:405–414. [PubMed: 17709559]

Liu Q, Wong-Riley MTT. Postnatal expression of neurotransmitters, receptors, and cytochrome oxidase in the rat pre-Bötzinger complex. J Appl Physiol. 2002; 92:923–934. [PubMed: 11842022]

Liu Q, Wong-Riley MTT. Postnatal changes in cytochrome oxidase expressions in brain stem nuclei of rats: implications for sensitive periods. J Appl Physiol. 2003; 95:2285–2291. [PubMed: 12909612]

Liu Q, Wong-Riley MTT. Developmental changes in the expression of GABAA receptor subunits alpha1, alpha2, and alpha3 in the rat pre-Botzinger complex. J Appl Physiol. 2004; 96:1825–1831. [PubMed: 14729731]

Liu Q, Wong-Riley MTT. Postnatal developmental expressions of neurotransmitters and receptors in various brain stem nuclei of rats. J Appl Physiol. 2005; 98:1442–1457. [PubMed: 15618314]

Liu Q, Wong-Riley MTT. Developmental changes in the expression of GABAA receptor subunits alpha1, alpha2, and alpha3 in brain stem nuclei of rats. Brain Res. 2006; 1098:129–138. [PubMed: 16750519]

Liu Q, Wong-Riley MTT. Postnatal changes in the expression of serotonin 2A receptors in various brain stem nuclei of the rat. J Appl Physiol. 2008; 104:1801–1808. [PubMed: 18420721]

Liu Q, Wong-Riley MTT. Postnatal changes in the expressions of serotonin 1A, 1B, and 2A receptors in ten brain stem nuclei of the rat: implication for a sensitive period. Neuroscience. 2010a; 165:61–78. [PubMed: 19800944]

Liu Q, Wong-Riley MTT. Postnatal changes in tryptophan hydroxylase and serotonin transporter immunoreactivity in multiple brainstem nuclei of the rat: implications for a sensitive period. J Comp Neurol. 2010b; 518:1082–1097. [PubMed: 20127812]

Liu Q, Wong-Riley MTT. Postnatal development of N-methyl-D-aspartate receptor subunits 2A, 2B, 2C, 2D, and 3B immunoreactivity in brain stem respiratory nuclei of the rat. Neuroscience. 2010c; 171:637–654. [PubMed: 20887777]

Liu Q, Lowry TF, Wong-Riley MTT. Postnatal changes in ventilation during normoxia and acute hypoxia in the rat: implication for a sensitive period. J Physiol. 2006; 577:957–970. [PubMed: 17038423]

Liu Q, Fehring C, Lowry TF, Wong-Riley MTT. Postnatal development of metabolic rate during normoxia and acute hypoxia in rats: implication for a sensitive period. J Appl Physiol. 2009; 106:1212–1222. [PubMed: 19118157]

Ludwig A, Uvarov P, Soni S, Thomas-Crusells J, Airaksinen MS, Rivera C. Early growth response 4 mediates BDNF induction of potassium chloride cotransporter 2 transcription. J Neurosci. 2011; 31:644–649. [PubMed: 21228173]

Lund IV, Hu Y, Raol YH, Benham RS, Faris R, Russek SJ, Brooks-Kayal AR. BDNF selectively regulates GABAA receptor transcription by activation of the JAK/STAT pathway. Sci Signal. 2008; 1:ra9. [PubMed: 18922788]

Maisonpierre PC, Belluscio L, Friedman B, Alderson RF, Wiegand SJ, Furth ME, Lindsay RM, Yancopoulos GD. NT-3, BDNF, and NGF in the developing rat nervous system: parallel as well as reciprocal patterns of expression. Neuron. 1990; 5:501–509. [PubMed: 1688327]

Marmigère F, Rage F, Tapia-Arancibia L. GABA-gluta-mate interaction in the control of BDNF expression in hypothalamic neurons. Neurochem Int. 2003; 42:353–358. [PubMed: 12470709]

Martin JL, Finsterwald C. Cooperation between BDNF and glutamate in the regulation of synaptic transmission and neuronal development. Commun Integr Biol. 2011; 4:14–16. [PubMed: 21509169]

Martinowich K, Lu B. Interaction between BDNF and serotonin: role in mood disorders. Neuropsychopharmacology. 2008; 33:73–83. [PubMed: 17882234]

Matsumoto T, Rauskolb S, Polack M, Klose J, Kolbeck R, Korte M, Barde YA. Biosynthesis and processing of endogenous BDNF: CNS neurons store and secrete BDNF, not pro-BDNF. Nat Neurosci. 2008; 11:131–133. [PubMed: 18204444]

Mizoguchi Y, Ishibashi H, Nabekura J. The action of BDNF on GABA(A) currents changes from potentiating to suppressing during maturation of rat hippocampal CA1 pyramidal neurons. J Physiol. 2003; 548:703–709. [PubMed: 12640007]

Narisawa-Saito M, Carnahan J, Araki K, Yamaguchi T, Nawa H. Brain-derived neurotrophic factor regulates the expression of AMPA receptor proteins in neocortical neurons. Neuroscience. 1999; 88:1009–1014. [PubMed: 10336116]

Nitta A, Fukumitsu H, Kataoka H, Nomoto H, Furukawa S. Administration of corticosterone alters intracellular localization of brain-derived neurotrophic factor-like immunoreactivity in the rat brain. Neurosci Lett. 1997; 226:115–118. [PubMed: 9159503]

Ogier M, Wang H, Hong E, Wang Q, Greenberg ME, Katz DM. Brain-derived neurotrophic factor expression and respiratory function improve after ampakine treatment in a mouse model of Rett syndrome. J Neurosci. 2007; 27:10912–10917. [PubMed: 17913925]

Onimaru H, Homma I. A novel functional neuron group for respiratory rhythm generation in the ventral medulla. J Neurosci. 2003; 23:1478–1486. [PubMed: 12598636]

Rekling JC, Feldman JL. Pre-Bötzinger complex and pacemaker neurons: hypothesized site and kernel for respiratory rhythm generation. Annu Rev Physiol. 1998; 60:385–405. [PubMed: 9558470]

Ribas-Salgueiro JL, Gaytán SP, Ribas J, Pásaro R. Characterization of efferent projections of chemosensitive neurons in the caudal parapyramidal area of the rat brain. Brain Res Bull. 2005; 66:235–248. [PubMed: 16023921]

Ricci A, Felici L, Mariotta S, Mannino F, Schmid G, Terzano C, Cardillo G, Amenta F, Bronzetti E. Neurotrophin and neurotrophin receptor protein expression in the human lung. Am J Respir Cell Mol Biol. 2004; 30:12–19. [PubMed: 12791675]

Rios M, Lambe EK, Liu R, Teillon S, Liu J, Akbarian S, Roffler-Tarlov S, Jaenisch R, Aghajanian GK. Severe deficits in 5-HT2A-mediated neurotransmission in BDNF conditional mutant mice. J Neurobiol. 2006; 66:408–420. [PubMed: 16408297]

Riva-Depaty I, Dubreuil YL, Mariani J, Delhaye-Bouchaud N. Eradication of cerebellar granular cells alters the developmental expression of trk receptors in the rat inferior olive. Int J Dev Neurosci. 1998; 16:49–62. [PubMed: 9664222]

Rivera C, Li H, Thomas-Crusells J, Lahtinen H, Viitanen T, Nanobashvili A, Kokaia Z, Airaksinen MS, Voipio J, Kaila K, Saarma M. BDNF-induced TrkB activation down-regulates the K+-Cl− cotransporter KCC2 and impairs neuronal Cl− extrusion. J Cell Biol. 2002; 159:747–752. [PubMed: 12473684]

Rivera C, Voipio J, Thomas-Crusells J, Li H, Emri Z, Sipilä S, Payne JA, Minichiello L, Saarma M, Kaila K. Mechanism of activity-dependent downregulation of the neuron-specific K-Cl cotransporter KCC2. J Neurosci. 2004; 24:4683–4691. [PubMed: 15140939]

Rocamora N, García-Ladona FJ, Palacios JM, Mengod G. Differential expression of brain-derived neurotrophic factor, neurotrophin-3, and low-affinity nerve growth factor receptor during the postnatal development of the rat cerebellar system. Brain Res Mol Brain Res. 1993; 17:1–8. [PubMed: 8381892]

Schinder AF, Berninger B, Poo M. Postsynaptic target specificity of neurotrophin-induced presynaptic potentiation. Neuron. 2000; 25:151–163. [PubMed: 10707980]

Schmid DA, Yang T, Ogier M, Adams I, Mirakhur Y, Wang Q, Massa SM, Longo FM, Katz DM. A TrkB small molecule partial agonist rescues TrkB phosphorylation deficits and improves

respiratory function in a mouse model of Rett syndrome. J Neurosci. 2012; 32:1803–1810. [PubMed: 22302819]

Small DL, Murray CL, Mealing GA, Poulter MO, Buchan AM, Morley P. Brain derived neurotrophic factor induction of N-methyl-D-aspartate receptor subunit NR2A expression in cultured rat cortical neurons. Neurosci Lett. 1998; 252:211–214. [PubMed: 9739998]

Smith JC, Morrison DE, Ellenberger HH, Otto MR, Feldman JL. Brainstem projections to the major respiratory neuron populations in the medulla of the cat. J Comp Neurol. 1989; 281:69–96. [PubMed: 2466879]

Smith JC, Ellenberger HH, Ballanyi K, Richter DW, Feldman JL. Pre-Bötzinger complex: a brain stem region that may generate respiratory rhythm in mammals. Science. 1991; 254:726–729. [PubMed: 1683005]

Smith JC, Butera RJ, Koshiya N, Negro CD, Wilson CG, Johnson SM. Respiratory rhythm generation in neonatal and adult mammals: the hybrid pacemaker-network model. Respir Physiol. 2000; 122:131–147. [PubMed: 10967340]

Tan J, Shepherd RK. Aminoglycoside-induced degeneration of adult spiral ganglion neurons involves differential modulation of tyrosine kinase B and p75 neurotrophin receptor signaling. Am J Pathol. 2006; 169:528–543. [PubMed: 16877354]

Thoby-Brisson M, Cauli B, Champagnat J, Fortin G, Katz DM. Expression of functional tyrosine kinase B receptors by rhythmically active respiratory neurons in the pre-Bötzinger complex of neonatal mice. J Neurosci. 2003; 23:7685–7689. [PubMed: 12930808]

Thoenen H, Zafra F, Hengerer B, Lindholm D. The synthesis of nerve growth factor and brain-derived neurotrophic factor in hippocampal and cortical neurons is regulated by specific transmitter systems. Ann N Y Acad Sci. 1991; 640:86–90. [PubMed: 1776765]

Tongiorgi E, Armellin M, Giulianini PG, Bregola G, Zucchini S, Paradiso B, Steward O, Cattaneo A, Simonato M. Brain-derived neurotrophic factor mRNA and protein are targeted to discrete dendritic laminas by events that trigger epileptogenesis. J Neurosci. 2004; 24:6842–6852. [PubMed: 15282290]

Van Bockstaele EJ, Pieribone VA, Aston-Jones G. Diverse afferents onverge on the nucleus paragigantocellularis in the rat ventrolateral medulla: retrograde and anterograde tracing studies. J Comp Neurol. 2004; 290:561–584. [PubMed: 2482306]

Wardle RA, Poo MM. Brain-derived neurotrophic factor modulation of GABAergic synapses by postsynaptic regulation of chloride transport. J Neurosci. 2003; 23:8722–8732. [PubMed: 14507972]

Wetmore C, Cao YH, Pettersson RF, Olson L. Brain-derived neurotrophic factor: subcellular compartmentalization and interneuronal transfer as visualized with anti-peptide antibodies. Proc Natl Acad Sci U S A. 1991; 88:9843–9847. [PubMed: 1946410]

Wong-Riley MTT, Liu Q. Neurochemical development of brain stem nuclei involved in the control of respiration. Respir Physiol Neurobiol. 2005; 149:83–98. [PubMed: 16203213]

Wong-Riley MTT, Liu Q. Neurochemical and physiological correlates of a critical period of respiratory development in the rat. Respir Physiol Neurobiol. 2008; 164:28–37. [PubMed: 18524695]

Xiong H, Futamura T, Jourdi H, Zhou H, Takei N, Diverse-Pierluissi M, Plevy S, Nawa H. Neurotrophins induce BDNF expression through the glutamate receptor pathway in neocortical neurons. Neuropharmacology. 2002; 42:903–912. [PubMed: 12069900]

Yoshii A, Constantine-Paton M. Postsynaptic BDNF-TrkB signaling in synapse maturation, plasticity, and disease. Dev Neurobiol. 2010; 70:304–322. [PubMed: 20186705]

Zec N, Kinney HC. Anatomic relationships of the human nucleus paragigantocellularis lateralis: a DiI labeling study. Auton Neurosci. 2001; 89:110–124. [PubMed: 11474639]

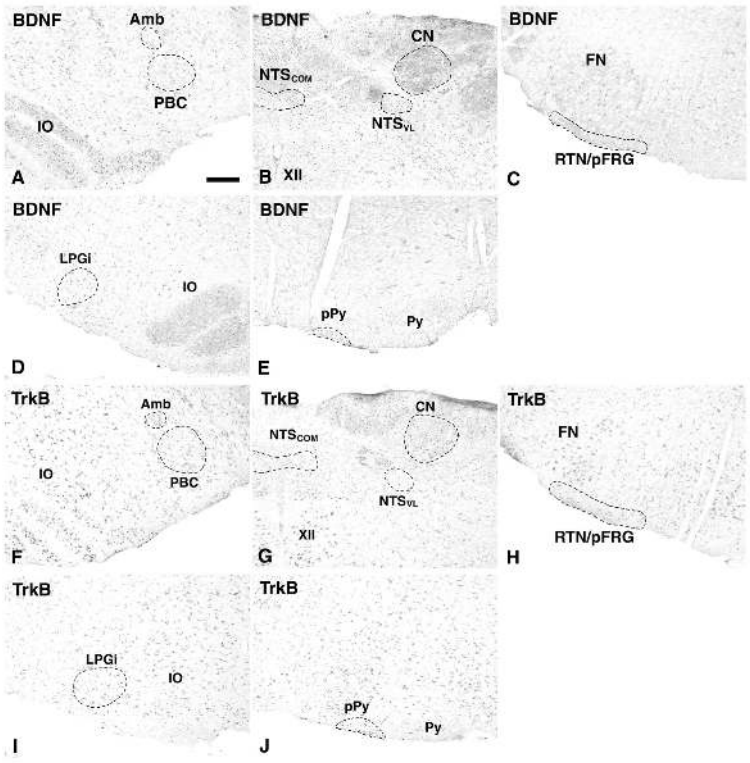

Figure 1.

Low-magnification photographs of rat brain stem sections at P7 reacted for brain-derived neurotrophic factor (BDNF) (A–E) and tyrosine protein kinase B (TrkB) receptor (F–J). Diagrammatic insets in Figures 2–5 and 7–10 indicate the location of each nucleus in cross-sections of the medulla. The other insets in these figures are higher magnifications of representative labeled neurons (indicated by arrows in the figures) highlighting the accumulation of immunoreaction product along the plasma membranes of the cell bodies or granular distribution of immunoreactive products in the cytoplasm (shown with arrowheads in the figures). XII, hypoglossal nucleus; Amb, nucleus ambiguus; CN, cuneate nucleus; FN, facial nucleus; IO, inferior olivary nucleus; LPGi, lateral paragigantocellular nucleus; NTS_{COM}, commissural subnucleus of the solitary tract nucleus; NTS_{VL}, ventrolateral subnucleus of the solitary tract nucleus; PBC, pre-Bötzinger complex; Py pyramidal tract; pPy, parapyramidal region; RTN/pFRG, retrotrapezoid nucleus/parafacial respiratory group. Scale bar = 200 □m.

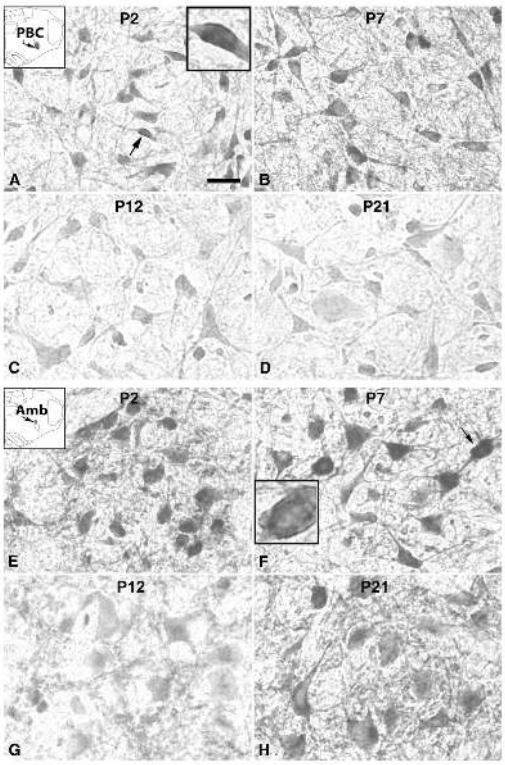

Figure 2.

BDNF-ir neurons and neuropil in the PBC (A–D) and Amb (E–H) at postnatal days P2 (A,E), P7 (B,F), P12 (C,G), and P21 (D,H). The expression of BDNF in both nuclei was relatively high at P2 and P7, but was markedly reduced at P12. At P21, the level remained low in the PBC, but was much higher in the Amb. Insets in A,F highlight plasma membrane labeling of BDNF-ir neurons. Scale bar 20 = □m (6.66 □m for insets).

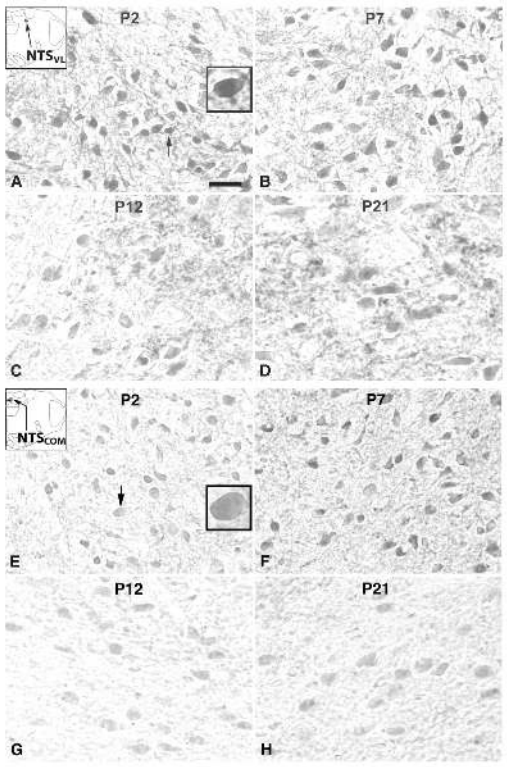

Figure 3.

BDNF-ir neurons and neuropil in the NTS_{VL} (A–D) and NTS_{COM} (E–H) at P2, P7, P10, and P21. BDNF expression in the NTS_{VL} and NTS_{COM} was relatively high at P2 and P7, but was significantly reduced at P12, followed by a relative plateau at P21. Insets in A,E highlight plasma membrane labeling of BDNF-ir neurons. Scale bar = 20 μm (6.66 μm for insets).

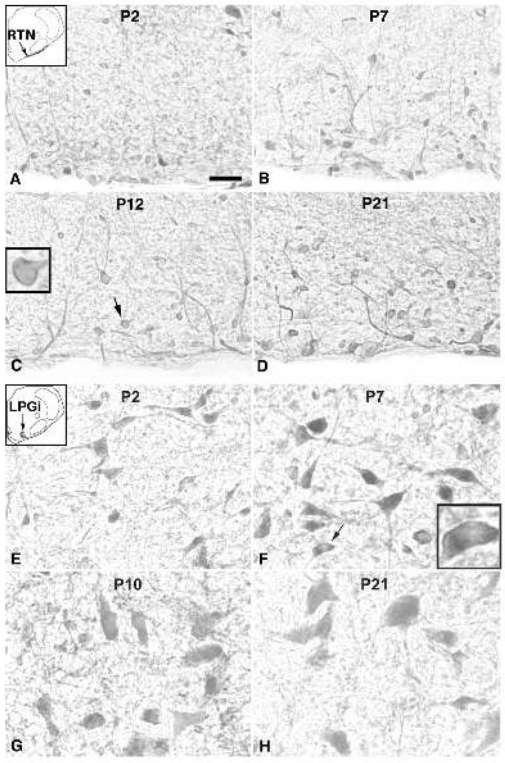

Figure 4.
BDNF-ir neurons and neuropil in the RTN/pFRG (A–D) and LPGi (E–H) at P2, P7, P12 (or P10 for LPGi), and P21. BDNF-ir in the RTN/pFRG exhibited comparable levels at P2, P7, and P21, but lower at P12, whereas that in the LPGi was relatively low at P2, increased significantly at P7 but fell at P10 and plateaued at P21. Insets in C,F highlight plasma membrane labeling of BDNF-ir neurons. Scale bar = 20 μm (6.66 μm for insets).

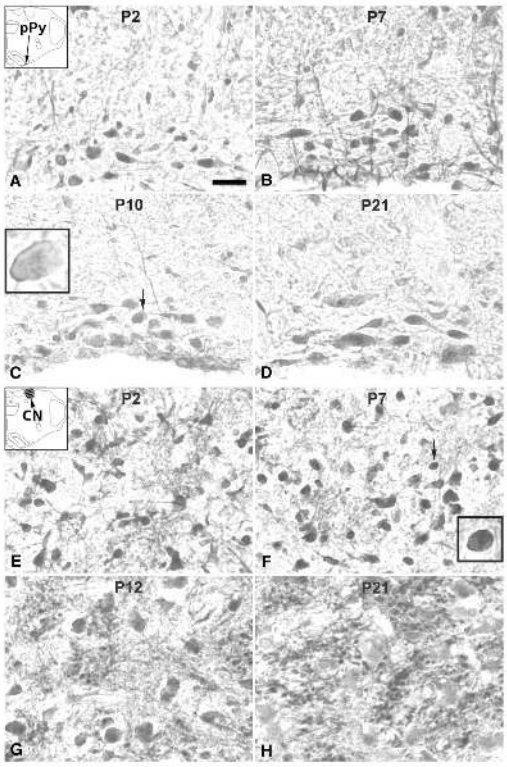

Figure 5.
BDNF-ir neurons and neuropil in the pPy (A–D) and CN (E–H) at P2, P7, P12 (or P10 for pPy), and P21. Immunoreactivity in the pPy increased at P7 but was reduced at P10, followed by a relative plateau at P21. BDNF-ir in neurons of the CN was relatively strong during the first 2 postnatal weeks but declined slightly in the third week. However, labeling in the neuropil was increased at P12 and thereafter, with distinct punctate or globular distribution (G,H). Insets in C,F highlight plasma membrane labeling of BDNF-ir neurons. Scale bar = 20 μm (6.66 μm for insets).

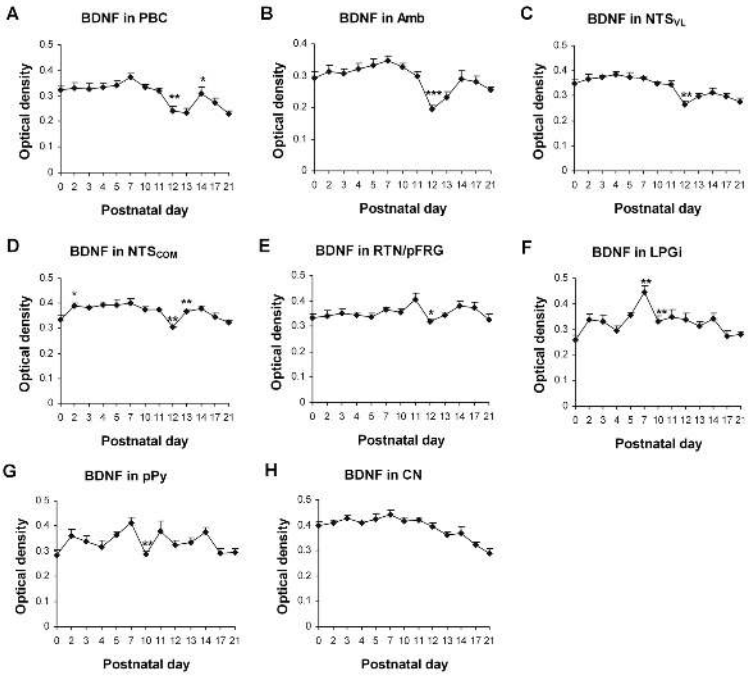

Figure 6.

Optical densitometric measurements of immunoreactive product for BDNF in individual neurons of the PBC (A), Amb (B), NTS_{VL} (C), NTS_{COM} (D), RTN/pFRG (E), LPGi (F), pPy (G), and CN (H) from P0 to P21. Data points are presented as mean ± SEM. Note that the values in the PBC, Amb, NTS_{VL}, NTS_{COM}, and RTN/pFRG were significantly reduced at P12, whereas those in the LPGi and pPy were significantly reduced at P10, after peaking at P7. The values in the CN was relatively high from P0 to P11, followed by a gradual decline thereafter. ANOVA yielded significant differences in the expression of BDNF among the ages in all eight nuclei examined ($P < 0.01$). Tukey's Studentized tests revealed significance between one age group and its immediately adjacent younger age group. *$P <$ 0.05; **$P < 0.01$; ***$P < 0.001$.

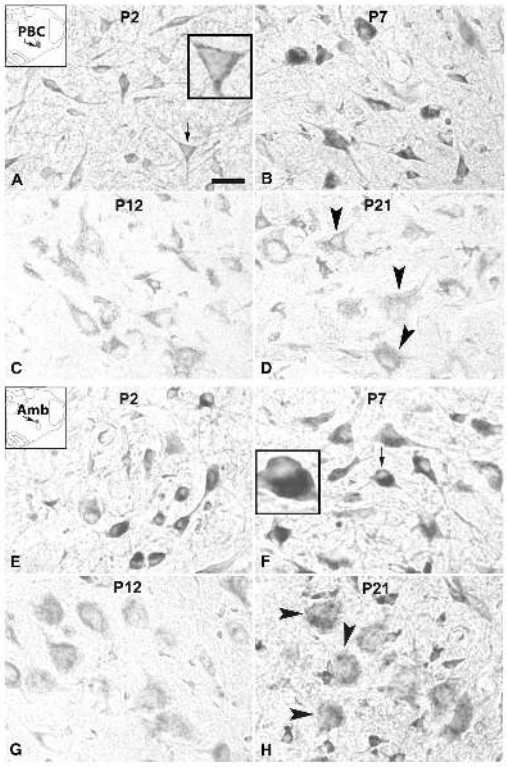

Figure 7.

TrkB-ir neurons and neuropil in the PBC (A–D) and Amb (E–H) at P2, P7, P12, and P21. In the PBC neurons, TrkB expression was low at P2, increased at P7, followed by a significant fall at P12 and a slightly higher level at P21. TrkB expression in Amb neurons was relatively high at P2 and P7, but decreased significantly at P12, with a return to a relatively high level at P21. Insets in A,F highlight plasma membrane labeling of TrkB-ir neurons. Arrowhead in D,H show the granular appearance of TrkB-ir after P10 as opposed to the more homogeneous appearance before P10. Scale bar = 20 □m (6.66 □m for insets).

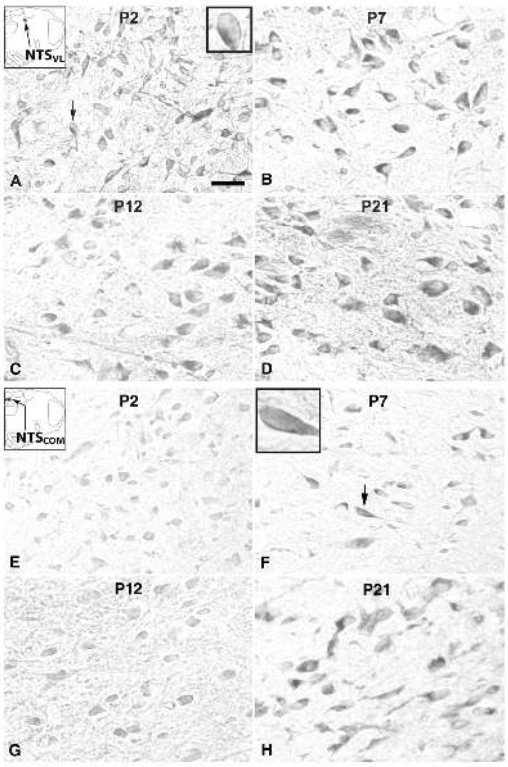

Figure 8.
TrkB-ir neurons and neuropil in the NTS_{VL} (A–D) and NTS_{COM} (E–H) at P2, P7, P12, and P21. Both NTS_{VL} and NTS_{COM} neurons exhibited low levels of TrkB-ir at P2, much higher levels at P7 followed by a striking reduction at P12, then returned to a high level at P21. Insets in A,F highlight plasma membrane labeling of TrkB-ir neurons. Scale bar = 20 μm (6.66 μm for insets).

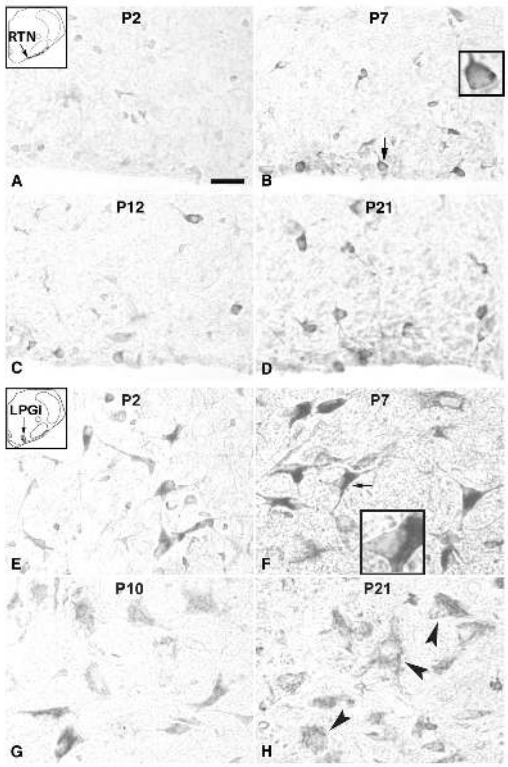

Figure 9.

TrkB-ir in the RTN/pFRG (A–D) and LPGi (E–H) at P2, P7, P12 (or P10 for LPGi), and P21. The level of TrkB in RTN/pFRG neurons was low at P2, relatively high at P7, significantly reduced at P12, and high again at P21. TrkB-ir in the LPGi neurons was low at P2, much increased at P7, followed by a significant reduction at P10 and a plateau at P21. Insets in B,F highlight plasma membrane labeling of TrkB-ir neurons. Arrowhead in H indicates the granular appearance of TrkB-ir in the LPGi after P10. Scale bar = 20 μm (6.66 μm for insets).

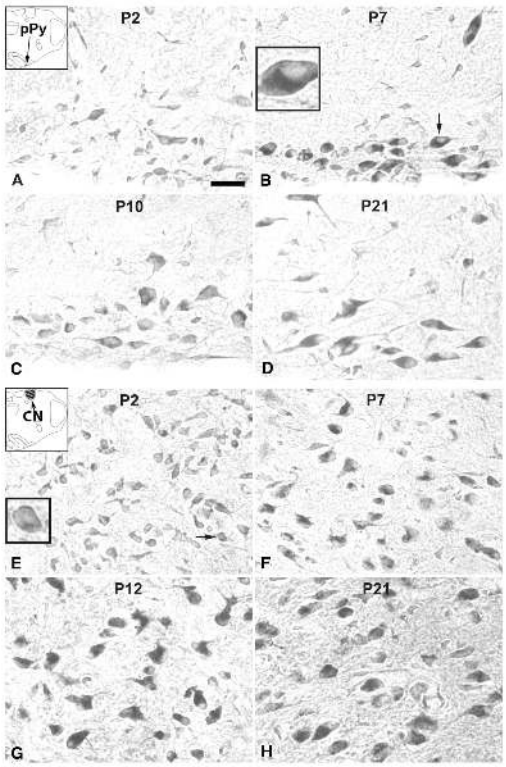

Figure 10.
TrkB-ir neurons and neuropil in the pPy (A–D) and CN (E–H) at P2, P7, P12 (or P10 for pPy), and P21. TrkB-ir in pPy neurons was low at P2, markedly increased at P7, followed by a significant decline at P10 and a comparable level at P21. In CN neurons, TrkB-ir was low at P2, increased gradually at P7 and P12, followed by a plateau at P21. Insets in B and E highlight plasma membrane labeling of TrkB-ir neurons. Scale bar = 20 μm (6.66 μm for insets).

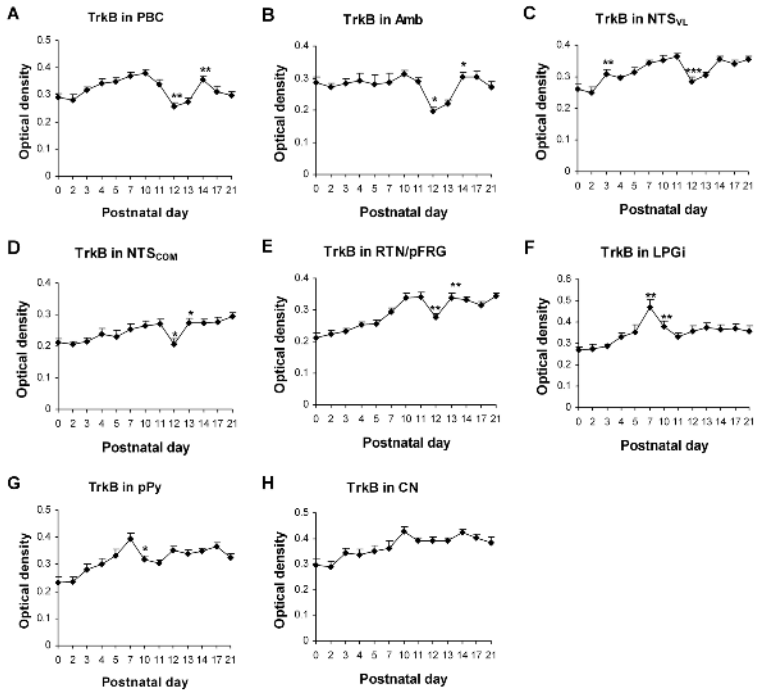

Figure 11.

Optical densitometric measurements of immunoreactive product for TrkB in individual neurons of the PBC (A), Amb (B), NTS_{VL} (C), NTS_{COM} (D), RTN/pFRG (E), LPGi (F), pPy (G), and CN (H) from P0 to P21. Data points are presented as mean ± SEM. Note that the values in all but the Amb were relatively low at P0–2, rose steadily to peak at P7 for LPGi and pPy, and at P10–11 for the other nuclei. A sudden and statistically significant reduction in TrkB-ir values occurred at P10 for LPGi and pPy, and at P12 for the PBC, Amb, NTS_{VL}, NTS_{COM}, and RTN/pFRG. These values rose 1 or 2 days later and plateaued thereafter until P21. In contrast, TrkB-ir values in the CN remained relatively high from P3 onward. ANOVA yielded significant differences in the expression of TrkB among the ages in all eight nuclei examined ($P < 0.01$). Tukey's Studentized tests revealed significance between one age group and its immediately adjacent younger age group. *$P < 0.05$; **$P < 0.01$; ***$P < 0.001$.

TABLE 1

Primary Antibodies Used

Antigen	Immunogen	Manufacturer, species, type, catalog number	Dilution Used
Brain-derived neurotrophic factor (BDNF)	Human BDNF, within an internal region of BDNF	Santa Cruz Biotechnology, (Santa Cruz, CA), rabbit polyclonal IgG, sc-546, N-20	1:100
Tyrosine protein kinase B or Tropomyosin-related kinase B (TrkB) receptor	Intracellular C-terminus of mouse TrkB (amino acids 794-808)	Santa Cruz Biotechnology, rabbit polyclonal IgG, sc-12, 794	1:1,000